Study on Deconvolution Algorithms for Optical Coherent Tomography

I-Chien Jan* Chih-Hsiung Chiu En-Kwung Tien Gwo-Jen Jan[1]

Department of Electrical Engineering, National Taiwan University, Taipei, Taiwan, 106 ROC
[1]*Graduate Institute of Electro-optical Engineering, National Taiwan University, Taipei, Taiwan, 106 ROC*

Received 23 February 2003; Accepted 21 May 2003

Abstract

Optical Coherence Tomography (OCT) is a novel tool for biomedical imaging in recent years. The noninvasive cross-section images have longitudinal resolution of a few micrometers, which is applicable to detect small organizations and structures, and the resolution is limited by the wavelength and spectrum bandwidth of the light source. Based on an interferometric OCT and following the coherence theory, a linear shift invariant system model describing coherent light specimen interactions in OCT is presented. In this study, the axial point spread function (PSF) is obtained, and the image of a double-cover-glass phantom was restored and enhanced the image sharpness by using the constrained iterative restoration (CIR) algorithm. Another deconvolution method, non-negativity and support constraints recursive inverse filtering (NAS-RIF) blind deconvolution algorithm, is also used in this study. In onion image, restored by using NAS-RIF algorithm, shows better quality than using iterative algorithm.

***Keywords*:** Optical coherence tomography (OCT), Point spread function, Deconvolution algorithm.

Introduction

Optical imaging technique can provide high resolution, noninvasive and non-contacted images, which are very suitable on biomedical imaging and physiological applications. Comparing with the most imaging tools in clinical medicine, including X-ray computer tomography (X-ray CT), ultrasound imaging, and magnetic resonance imaging (MRI), the micrometer to sub-micrometer resolution, which is very needed in cellular-level studying, is the most advantage of optical imaging tools. Although the micrometer-resolution of optical imaging can provide fine structural information of cells and early diagnostic studies on pathological changes, the absorption and scattering of photons in biomedical tissues, which downgrade the penetration depth very much, still remain great problems in biomedical imaging applications. When the probing photons of wavelength in visible and ultraviolet bands, the photon absorption will decrease the probing depth very much. On the other hand, photons of wavelength longer than 2500 nm (near infrared, NIR) will be absorbed by the oscillation of water molecules, which not only decrease the penetration depth but also cause heat injuries on tissues. Consequently, the most suitable wavelength of optical probes in biomedical applications is between 600 to 1300 nm [1-2]. However, even though the absorption is low, but the scattering problem appears and making the difficulty on tissue imaging and position measuring. Therefore, some techniques on back-scattering light were studied and developed, include the optical coherence tomography.

Optical coherence tomography (OCT), which was first introduced by J. G. Fujimoto in 1991, is a novel optical imaging technique that can provide optical cross-section images of materials and biological tissues with micrometer-resolution [3]. Basically, OCT relies on the principle of low coherence interferometer (LCI), which used to be the measuring tool of thin film thickness and the break point of optical communication devices [4, 5]. The accuracy positioning ability of LCI made itself as a powerful tool of depth measurement applied on biological tissues, and with transverse scanning, one can get two-dimensional OCT images easily based on the LCI architecture. Since the very beginning of its appearance, OCT has been thought as a high potential imaging tool in biological and medical applications [6]. The longitudinal resolution is determined by the short-time interference characteristic of a broadband light source. Therefore, OCT have longer probing depth on biomedical tissues than conventional optical microscopes or confocal microscopes have. For example, OCT can measure a 2-cm deep micro-image in transparent tissues like eyes [7], and it can also perform 1 to 2-mm deep imaging in highly scattered media like skin [8].

* Corresponding author: I-Chien Jan
Tel: +886-2-23635251 ext.421; Fax: +886-2-23638247
E-mail: ijjan@pchome.com.tw

The system performance of OCT is highly depends on optical light source and the method of modulation. The transverse resolution depends on the diameter of focusing spot, while the longitudinal resolution depends on the optical coherence length of the light source. In the meanwhile, the signal to noise ratio and sensitivity depend on the intensity and power stability of the light source, and the imaging speed is determined by the modulation method [9]. By using a 10-mW super-luminescence diode (SLD) as the light source, one can get 20-μm longitudinal resolution; with a 100-mW Ti:sapphire mode-locked laser, the longitudinal resolution can down to 2-μm level [10]. The most usual modulation method in OCT system is displacement modulation performed by stepping motors or magnetic speakers. In 1998, the first phase-retarded modulation method in OCT was introduced, that makes the imaging speed of OCT pushed to a few tens frames per second and also a big step toward the practical application on clinical medicine [11].

Although we have set up an OCT system in 2001 in our laboratory, the low-cost equipments limited the system performance. Besides improving the image quality and resolution by hardware upgrade, the image processing technique can be also applied to upturn OCT images. Because the longitudinal resolution depends on the coherence of light source, we can get the one-dimensional PSF on the longitudinal axis. By performing some deconvolution algorithms, we can improve the image quality and longitudinal resolution of OCT images, which are convoluted with real images and the PSF. The deconvolution method can also eliminate some image distortions that come from the coherent character of the light source. In this study, we measure the axial PSF, and apply a constrained iterative restoration (CIR) algorithm and a non-negativity and support constraints recursive inverse filtering (NAS-RIF) blind algorithm to perform image deconvolution [11, 12]. Furthermore, we compare these two methods to confer the most proper deconvolution method applied on OCT images.

Methods

OCT system

The principle of OCT is based on the LCI, which can be illustrated with a Michelson interferometer shown in Figure 1. Optical beam coming from the light source (LS) is divided by a beamsplitter and then reflected by mirrors M_1 and M_2. The interferometric signal is detected by a photo-detector (PD). If we define the intensity of the two reflected beams as I_1 and I_2, then the signal intensity detected by PD can be described as [13]

$$I_d = I_1 + I_2 + 2\sqrt{I_1 I_2}\,\mathrm{Re}\{\gamma_{12}(\tau)\} \tag{1}$$

where

$$\gamma_{12}(\tau) = \frac{\int_{-\infty}^{\infty} E_1(t)E_2^{*}(t-\tau)dt}{\sqrt{\int_{-\infty}^{\infty} E_1(t)E_1^{*}(t)dt \int_{-\infty}^{\infty} E2(t)E2^{*}(t)dt}} = \frac{\Gamma_{12}(\tau)}{\sqrt{I_1 I_2}} \tag{2}$$

$\gamma_{12}(\tau)$ is called the degree of coherence, and $\Gamma_{12}(\tau)$ is the coherence function. When the optical path difference $\tau = 0$, $\gamma_{12}(\tau)$ and the interferometric signal become maximum value. Define FWHM of $[\gamma(\tau)]$ as coherence time τ_c

$$\frac{\gamma(\frac{\tau_c}{2})}{\gamma(0)} = \frac{\Gamma(\frac{\tau_c}{2})}{\Gamma(0)} = \frac{1}{2} \tag{3}$$

Multiplied by the speed of light c, the optical coherence length $l_c = c\tau_c$, and the relationship between l_c and the wavelength λ is described as

$$l_c = \frac{4\ln 2}{\pi}\frac{\lambda^2}{\Delta\lambda} \tag{4}$$

and the longitudinal resolution of OCT defined as R_l [14]

$$R_l = \frac{2\ln 2}{\pi}\frac{\lambda^2}{\Delta\lambda} \tag{5}$$

The experimental set-up of our OCT system is shown in Figure 2. We use a 2.5-mW SLD as the light source, with center wavelength at 811 nm and 19-nm bandwidth. The reference mirror is actuated by a piezoelectric tranlational stage with constant speed, and two stepping motors, controlled by a PC via IEEE-488 interface, actuate the sample stage. The optical signal detected by PD is demodulated by a lock-in amplifier, and then fed into PC via a 16-bit A/D converter. The signal read-out and the stage controlling are all done with a LabVIEW program to make it an automatic imaging system.

Deconvolution methods

The interferometric distortion of OCT image comes from the convolution of all detected signal with different optical path (within the coherence length). Therefore, we choose deconvolution algorithms to image restoration. Constrained

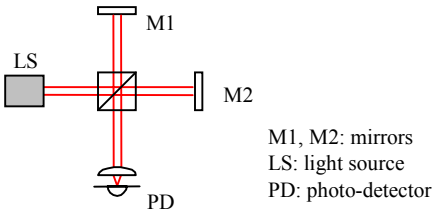

Figure 1. Schematic diagram of a Michelson interferometer.

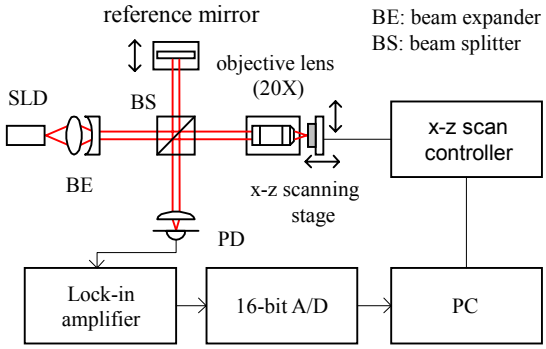

Figure 2. Schematic diagram of our OCT system.

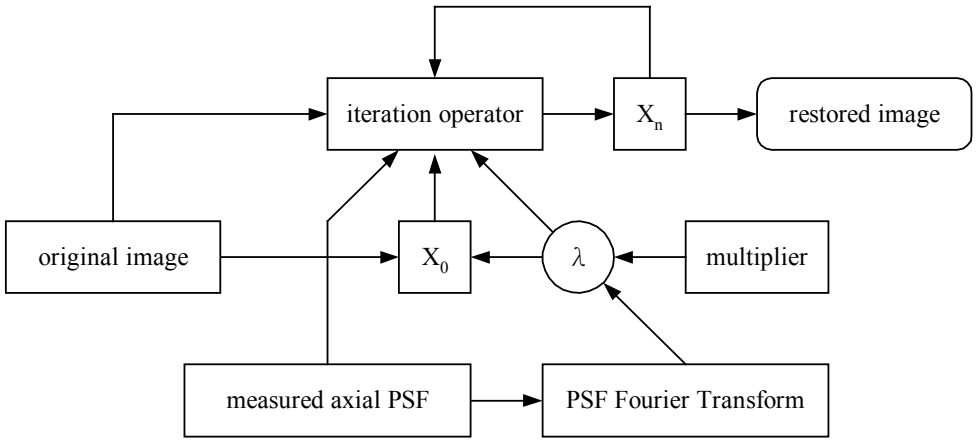

Figure 3. Schematic illustration of constrained iterative restoration algorithm.

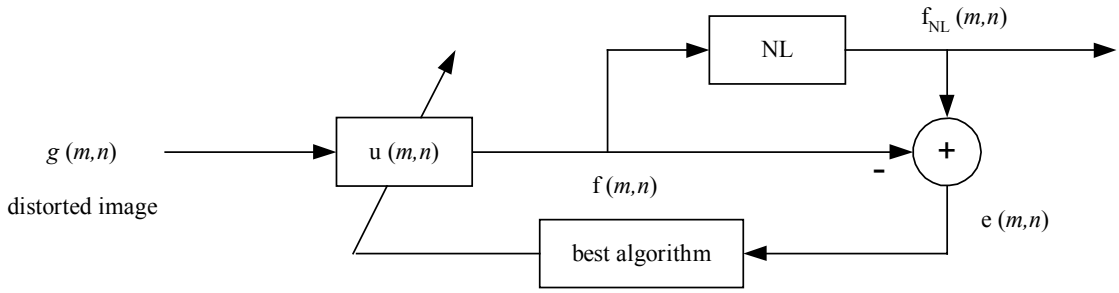

Figure 4. Schematic illustration of non-negativity and support constraints recursive inverse filtering algorithm.

iterative restoration (CIR) algorithm [15], one of non-blind one-dimensional deconvolution method, is very suitable for OCT image restoration, since the measurement of axial PSF is much easier than that of transverse PSF in OCT system. On the other hand, non-negativity and support constraints recursive inverse filtering (NAS-RIF) algorithm is a blind deconvolution method, which does not need the PSF to perform the image restoration [16].

The schematic illustration of CIR algorithm is shown in Figure 3. The principle of CIR algorithm can start from a simple iterative equation [15]

$$x_{k+1} = Fx_k \tag{6}$$

where F is the iteration operator. When k approaches infinity, x_k will converge to a singular solution. If we take the difference between x_k and the exact solution x, then the maximum value of k can be determined. Therefore, the F operator is the kernel of CIR. That means F should be selected to make the difference between x_k and x become smaller after once and once in the iteration sequence, and the constrain of this algorithm is the key to converge the iteration. If we write down an iteration form like this

$$x_{k+1} = Cx_k + \lambda(y - h * Cx_k) \tag{7}$$

where y as the measured value from OCT system, λ as a parameter, h as the PSF, and C as a constrained operator. Usually we start with $x_0 = \lambda y$. By selecting a proper value of λ, the iteration would be convergent. The constrain of the parameter λ is

$$0 < \lambda < \frac{2}{\max_{\omega}[H(e^{j\omega T})]} \tag{8}$$

where $\max_{\omega}[H(e^{j\omega T})]$ comes from the Fourier transform. The convergence constrains is that the spectrum of the light source must as a Gaussian, and which is conformable to our system.

In contrast with CIR, NAS-RIF algorithm does not need the PSF as a beginning guess, and has good character in iteration convergence. The cost function of NAS-RIF is convex, that means one can get the global minimum value through this method. The schematic illustration of NAS-RIF algorithm is shown in Figure 4. In the illustration, u (m, n) is an adjustable filter, g (m, n) is the distorted image, and f (m, n) is the result of g (m, n) through $u(m, n)$. *NL* is a nonlinear filter defined as [16]

$$f_{NL}(m,n) = \begin{cases} f(m,n), & \text{if } (m,m) \in D_{\sup} \\ L_B, & \text{if else} \end{cases} \tag{9}$$

where D_{sup} define the region of support (ROS) and L_B as the pixel value of background. An error function e (m, n), equaling to the difference between $f_{NL}(m, n)$ and f (m, n), can adjust the value of u (m, n). To optimize the algorithm, the cost function is considered as

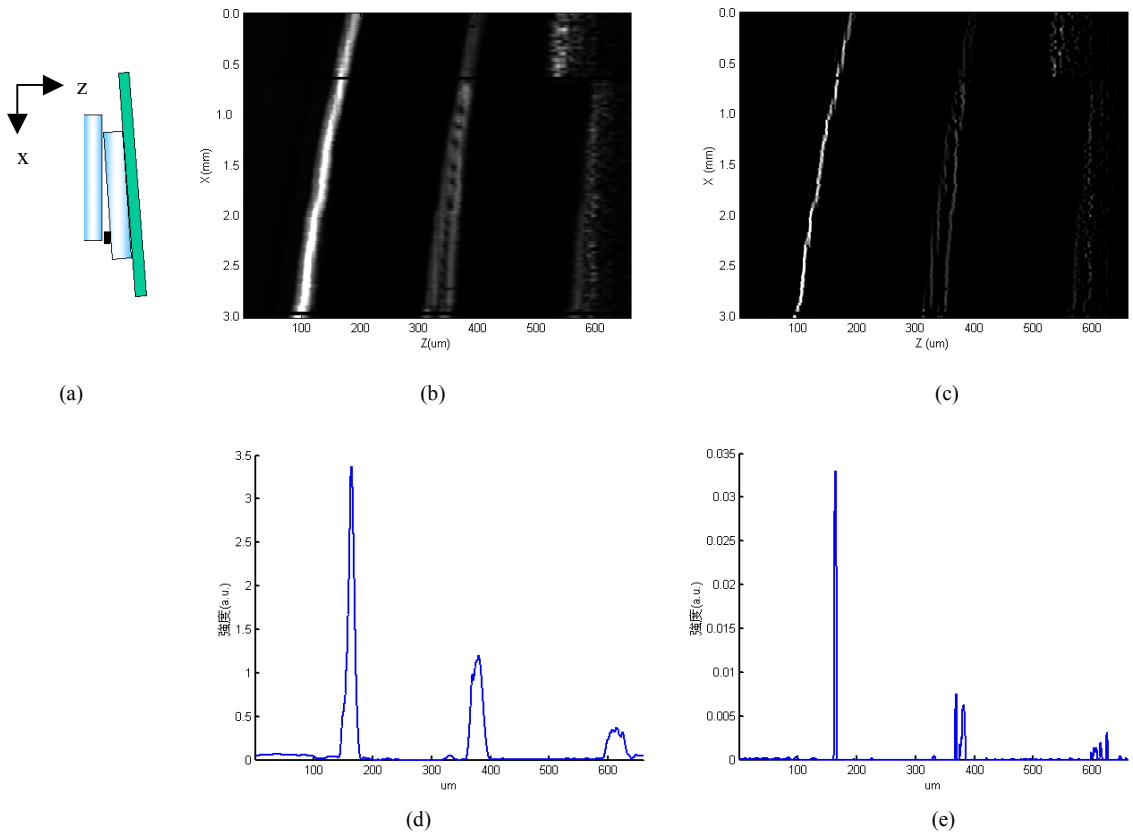

Figure 5. (a) Schematic diagram of the double cover glass phantom, (b) the OCT image and (c) the CIR result after 30-time iteration. The profile of (b) and (c), with sampling position marked on the figures, are shown in (d) and (e).

$$J(u)=\sum e^2(m,n)+\gamma\left[\sum u(m,n)-1\right]^2$$
$$=\sum_{(m,n)\in D_{\sup}} f^2(m,n)\left[\frac{1-\mathrm{sgn}(f(m,n))}{2}\right]+\sum_{(m,n)\notin D_{\sup}}\left[f(m,n)-L_B\right]^2$$
$$+\gamma\left[\sum_{\forall(m,n)} u(m,n)-1\right]^2 \qquad (10)$$

only when all L_B becomes to zero, γ has non-zero value. The optimization of the filter u (m, n) is to minimize the value of cost function J (u). The function sgn (f) is defined as

$$\mathrm{sgn}(f)=\begin{cases}1, & \text{if } f>0\\ -1, & \text{if else}\end{cases} \qquad (11)$$

Results and Discussion

The OCT system is constructed as Figure 2, and the resolution test shows the system provides 4-μm transverse resolution and 17-μm longitudinal resolution. By scanning a reflective mirror several times, we take the average PSF with a Gaussian fitting result as the PSF along the longitudinal axis

$$PSF=2.8e^{-\frac{1}{2}(\frac{\Delta l}{78})^2} \qquad (12)$$

Δl is the distance between each sampling point, with the modulation speed in our system, Δl equals to 0.11μm.

To perform the test of image restoration, we design a testing phantom shown in Figure 5 (a). The phantom is constructed of two cover glass and putting some plastic tape between the glasses. Make the contacting point as tight as could, and the distance between the two glasses is getting lager from the contacting point to the other end. The scanning coordinates are also shown in the figure, the raw scanning result is shown in Figure 5 (b). By 30 times iteration of CIR algorithm, the deconvolution image is shown in Figure 5 (c). The interfaces are well resolved in the CIR restored image, and the improvement can be clearly compared in the profile diagram shown in Figure 5 (d) and (e). We also apply the NAS-RIF method, however, it does not improve the axial resolution as well as CIR algorithm does (not shown in here).

Beside the testing phantom, we use onion tissue as biological sample to test the performance of the OCT system and the deconvolution methods. The onion tissue image by OCT is shown in Figure 6 (a). The top is the interface between air and the onion skin, and as deeper it goes, the signal is getting smaller. The image contrast is about 70 dB, SNR is about 40 to 65 dB. The CIR and NAS-RIF algorithms are also applied, and the results are shown in Figure 6 (b) and (c).

Comparing with the raw image, both of the deconvolution images show more features of the onion cells. However, the restored image of CIR becomes more fractional than NAS-RIF. The discontinuity may comes from the slight index changing in the tissue or just from the noise, but it still sharpens the edge and makes the image becomes more clear. On the other hand the restored image by NAS-RIF method improves both the

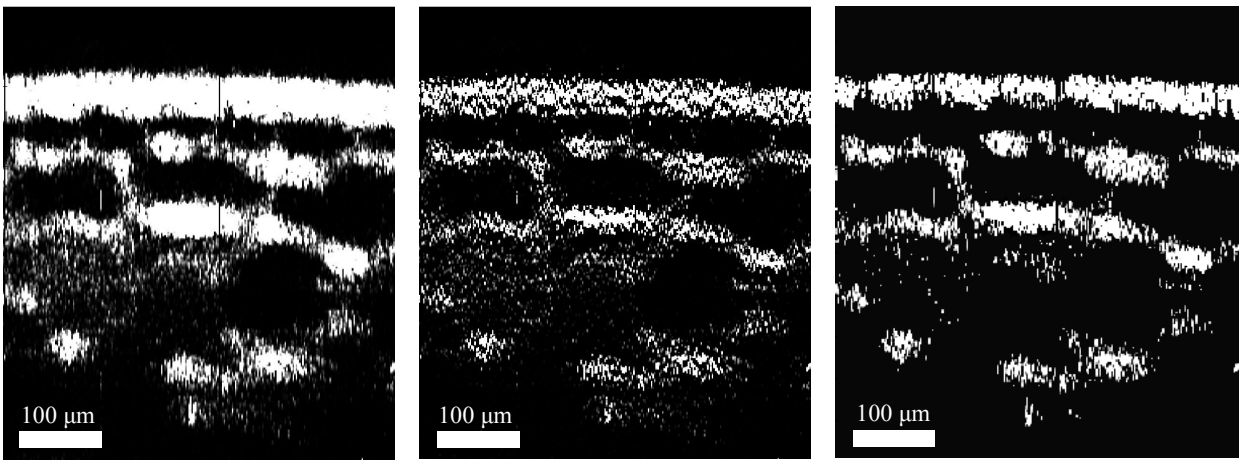

(a) (b) (c)

Figure 6. (a) OCT image of onion tissue, (b) CIR deconvolution result after 30-time iteration and (c) the NAS-RIF result.

image quality and the resolution indeed. The algorithm character of the NAS-RIF method can explain the result. Because the NAS-RIF does not rely on PSF to perform deconvolution, it searches proper filter by a given region of support (ROS). The result conforms with the ROS constrain but not the PSF, that will make it more tolerant to image noises. Nevertheless, CIR depends on PSF very much, and performs the same deconvolution on noisy regions. Like the PSF to CIR method, the selection of ROS will affect the restoration power very much in the NAS-RIF method.

Conclusion

In this study, we build a low-cost OCT system based on interferometric architecture with low coherent light source. The system provides 17-μm longitudinal and 4-μm transverse resolutions. By measuring cover glass phantom and biological sample, the system is verified to perform biomedical imaging. Two deconvolution methods are applied to restore OCT images. The constrained iterative restoration (CIR) algorithm can improve the longitudinal resolution in multi-interface image. On the other hand, the non-negativity and support constraints recursive inverse filtering (NAS-RIF) algorithm can improve image quality in the biological tissue images.

Acknowledgement

We would like to thank the National Science Council, R.O.C., for supporting the grant under contract number NSC 91-2213-E-002-085. The authors also thank Mr. B. C. Chen for his technical assistance.

References

[1] M. S. Patterson, B. Chance, and B. C. Wilson, "Time Resolved Reflectance and Transmittance for the Non-invasive Measurement of Tissue Optical Properties," *Applied Optics*, 28: 2331-2336, 1989.

[2] W. F. Cheong, S. A. Prahl, and A. J. Welch, "A Review of the Optical Properties of Biological Tissues," IEEE J. *Quantum Electron*, 26: 2166-2185, 1990.

[3] D. Huang, E. A. Swanson, C. P. Lin, J. S. Schuman, W. G. Stinson, W. Chang, M. R. Hee, T. Flotte, K. Gregory, C. A. Puliafito, and J. G. Fujimoto, "Optical Coherence Tomography", *Science*, 254: 1178-1181, 1991.

[4] P. A. Flourney, "White-light Interferometric Thickness Gauge", *Applied Optics*, 11: 1907-1915, 1972.

[5] R. C. Youngquist, S. Carr, and D. E. N. Davies, "Optical Coherence-domain Reflectometry: a New Optical Evaluation Technique", *Optics Letters,* 12: 158-160, 1987.

[6] A. F. Fercher, K. Mengedoht, and W. Werner, "Eye-length Measurement by Interferometry with Partially Coherent Light", *Optics Letters*, 13: 1867-1869, 1988.

[7] M. R. Hee, J. A. Izatt, E. A. Swanson, D. Huang, C. P. Lin, J. S. Schuman, C. A. Puliafito, and J. G. Fujimoto, "Optical Coherence Tomography of the Human Retina", *Archives of Ophthalmology*, 113: 326-332, 1995.

[8] J. M. Schmitt, M. Yadlowsky, and R. F. Bonner, "Subsurface Imaging in Living Skin with Optical Coherence Tomography", *Dermatology*: International Journal for Clinical and Investigational Dermatology, 191: 93-98, 1995.

[9] J. Szydlo, N. Delachenal, R. Giannini, R. Walti, H. Bleuler, and R. Salathe, "Air-turbine Driven Optical Low-Coherence Reflectometry at 28.6-kHz Scan Repetition rate", *Optics Communications*, 154: 1-4, 1998.

[10] B. Bouma, G. J. Tearney, S. A. Boppart, M. R. Hee, M. E. Brezinski, and J. G. Fujimoto, "High-Resolution Optical Coherence Tomographic Imaging Using a Mode-Locked Ti-Al2O3 Laser Source," Optics Letters 20: 1486-1488, 1995.

[11] C. B. Su, "Achieving Variation of the Optical Path Length by a Few Millimeters at Millisecond Rates For Imaging of Turbid Media and Optical Interferometry", *Optics Letters*, 22: 665-667, 1997.

[12] G. J. Tearney, M. E. Brezinski, B. E. Bouma, S. A. Boppart, C. Pitris, J. F. Southern, and J. G. Fujimoto, "In Vivo Endoscopic Optical Biopsy with Optical Coherence Tomography", *Science*, 276: 2037-2039, 1997.

[13] R, Guenther, "Modern Optics", *New York: Wiley*, ch8: 299-307, 1990.

[14] J. M. Schmitt, "Optical Coherent Tomography (OCT): A Review", *IEEE J. of Selected Topics in Quantum Electron*, 5: 1205-1212, 1999.

[15] R.W. Schafer, R. M. Mersereau, and M. A. Richards, "Constrained Iterative Restoration Algorithms", *Proc. IEEE,* 69: 432-450, 1981.

[16] D. Kundur and D. Hatzinakos, "On the Use of Lyapunov Criteria to Analyze the Convergence of Blind Deconvolution Algorithms", *IEEE Trans. signal processing,* 46: 2918-2925, 1998.